Molecular high-order-harmonic generation due to the recollision mechanism by a circularly polarized laser pulse

Xiaosong Zhu,[1] Xi Liu,[1] Yang Li,[1] Meiyan Qin,[1] Qingbin Zhang,[1] Pengfei Lan,[1] and Peixiang Lu[1,2,*]

[1]*Wuhan National Laboratory for Optoelectronics and School of Physics, Huazhong University of Science and Technology, Wuhan 430074, China*

[2]*Laboratory of Optical Information Technology, Wuhan Institute of Technology, Wuhan 430073, China*

(Received 26 November 2014; revised manuscript received 9 February 2015; published 24 April 2015)

High-order-harmonic generation (HHG) from small linear molecules driven by a circularly polarized laser pulse (CPLP) is investigated. It is found that the obtained high-order harmonics are more pronounced than those from reference atoms with equal ionization potential driven by the same CPLP. By analyzing the dependence of the cutoff position on laser parameters and calculating the recollision trajectories, it is shown that this molecular HHG originates from the recollision mechanism, instead of the bound-bound transition mechanism found to be responsible for molecular HHG by CPLP in earlier works. A semiclassical model is used to analyze the HHG process and discuss the origin of the higher efficiency of molecular HHG. It is found that the higher HHG efficiency for molecules is mainly contributed in the recombination step and at least partly due to the higher recollision probability of continuum electrons.

DOI: 10.1103/PhysRevA.91.043418 PACS number(s): 32.80.Rm, 42.65.Ky

I. INTRODUCTION

When atoms and molecules are exposed to intense laser irradiation, high-order harmonics are generated. The high-order-harmonic generation (HHG) has been an attractive topic in the past two decades for its potential application of producing coherent attosecond pulses in the XUV regime [1–9] and self-probing of molecules allowing a combination of attosecond and Ångström resolutions [10–17]. The generation of high-order harmonics driven by a linearly polarized laser pulse (LPLP) can be explained by the semiclassical recollision mechanism [18–20], where the HHG process consists of three steps: (i) an atom or molecule emits its electron to a continuous state, (ii) the electron is accelerated in the laser field, and (iii) the accelerated electron recombines with the parent ion and a high energy photon is radiated. This model can be supported by two simple experimental observations. First, the cutoffs in the harmonic spectra locate at the photon energy of $3.17U_p + I_p$, where I_p is the ionization potential of the target atom or molecule, $U_p = E_0^2/4\omega_0^2$ is the ponderomotive energy of the ionized electron, and E_0 and ω_0 are the peak amplitude and frequency of the laser field, respectively [21,22]. This is consistent with the semiclassical calculation that the maximum kinetic energy of the recolliding electron accelerated by LPLP is $3.17U_p$. Second, if the driving laser deviates from linear polarization, the HHG efficiency decreases with the increase of the ellipticity, because the ionized electrons are transversely accelerated and may miss the core [23–25].

Plenty of experiments and simulations show that the behaviors of atoms and molecules are similar in HHG driven by LPLP or an elliptically polarized laser pulse with small ellipticity. However, it is found that their behaviors are far different if the laser pulse is circularly polarized. For atoms, the HHG efficiency is quite low. While for molecules (such as benzene, and also thin crystals and nanostructures) possessing Nth order rotational symmetry, high-order harmonics with frequencies $\Omega = \omega, (lN \pm 1)\omega, l = 1,2,\ldots,$ are efficiently generated [26–31]. The cutoff position is not at $3.17U_p + I_p$ and depends linearly on the electric field and the molecular dimensions [28]. Previous investigations based on one- or multiple-electron 2D/3D theoretical methods all show that this kind of molecular HHG originates from bound-bound transitions [26,29–31]. This mechanism also dominates the HHG when the laser polarization deviates from the "ideal" circular one by about 5% [30].

Coming back to the recollision mechanism, the HHG based on recollision is still an efficient mean of obtaining harmonics of very high orders, because of the advantageous cutoff position scaling compared to bound-bound transitions, such that many works have taken advantage of the geometrical structure of the considered molecules to induce recollision and extend the cutoff even higher [32–34]. Therefore, the recollision process under a circularly polarized laser pulse (CPLP) and the recollision induced HHG from (pre-excited) atomic systems are also investigated [35–38]. These works show that the recollision under CPLP does occur and has a significant effect on the recollision-driven processes (such as nonsequential double ionization and HHG). Then, considering molecular targets with small dimension and the mid-infrared driving lasers, where the quiver radius is much larger than the internuclear distance, the geometrical tricks become less important and the molecular system is much like an atomic target at the scale of the laser induced electronic dynamics. In this case, the findings from atoms may also exist for small molecules, and on the other hand, some new features are expected due to the nonspherical structure of molecules. This can be studied by comparing the HHG from small molecules and atoms.

In this work we investigate the HHG driven by CPLP from small linear molecules such as CO_2 and N_2. Different from the previously known "symmetry-allowed harmonics" based on bound-bound transitions, by analyzing the dependence of the cutoff position on laser parameters and calculating the recollision trajectories, it is shown that these molecular HHG are due to the recollision mechanism. Moreover, the

*Corresponding author: lupeixiang@mail.hust.edu.cn

high-order harmonics generated from molecules are more pronounced than those generated from atoms with an equal ionization potential with CPLP. It is found that the higher efficiency is mainly contributed in the recombination step and is at least partly due to the higher recollision probability for molecules. Since this HHG process involves the unique recollision mechanism under a circularly polarized laser field, it will stimulate new potential applications, such as offering an ideal framework for study of strong-field dynamics [37] and (one-shot) imaging or structure detection of molecules with all optical methods [39–42].

II. THEORETICAL MODEL

In this work we investigate the interaction of molecules and atoms with laser pulses by solving a two-dimensional single-active-electron (SAE) time-dependent Schrödinger equation (TDSE) (atomic units are used throughout this paper unless otherwise stated):

$$i\frac{\partial}{\partial t}\psi(\mathbf{r},t) = \hat{H}(\mathbf{r},t)\psi(\mathbf{r},t) \tag{1}$$

numerically. The Hamiltonian reads

$$\hat{H}(\mathbf{r},t) = -\frac{1}{2}\nabla^2 + V(\mathbf{r}) + \mathbf{r}\cdot\mathbf{E}(t). \tag{2}$$

$\mathbf{E}(t)$ is the electric field and $V(\mathbf{r})$ is the model potential of the system. For molecules we employ the SAE soft-core potential in the form of [16,43]

$$V(\mathbf{r}) = -\sum_j \frac{Z_j^\infty + \left(Z_j^0 - Z_j^\infty\right)\exp\left(-\mathbf{r}_j^2/\sigma_j^2\right)}{\sqrt{\mathbf{r}_j^2 + a_j^2}}. \tag{3}$$

The subscript $j = 1,\ldots,N$ labels the nuclei at fixed positions $\boldsymbol{\rho}_j$ and $\mathbf{r}_j = \mathbf{r} - \boldsymbol{\rho}_j$. The numerator $Z_j^\infty + (Z_j^0 - Z_j^\infty)\exp(-\mathbf{r}_j^2/\sigma_j^2)$ is the position-dependent screened effective charge for the jth nucleus, where Z_j^∞ denotes the effective nuclear charge of the nucleus j as seen by an electron at infinite distance and Z_j^0 is the bare charge of nucleus j. Parameter σ_j characterizes the decrease of the effective charge with the distance to the nucleus. a_j is the soft-core parameter. For the simulations of CO_2 and N_2, the values of the parameters are given following Ref. [43] as summarized in Table I, where the values of Z_j^∞ were derived from a Mulliken analysis carried out in *ab initio* study.

The TDSE is solved using the split-operator method [44]. The initial states are obtained by solving TDSE with imaginary-time propagation [43,45], where the excited states

TABLE I. Values of all parameters used for soft-core potentials of CO_2 and N_2 [43].

Molecule	CO_2			N_2	
Nucleus	O	C	O	N	N
a_j (a.u.)	1.0	1.0	1.0	1.2	1.2
σ_j^2 (a.u.)	0.577	0.750	0.577	0.700	0.700
Z_j^0	8	6	8	7	7
Z_j^∞	0.173	0.654	0.173	0.500	0.500

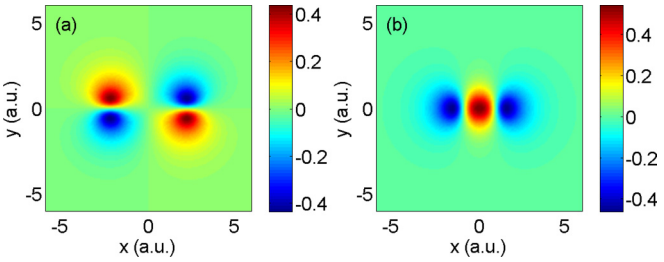

FIG. 1. (Color online) Initial states for (a) CO_2 and (b) N_2 obtained by solving TDSE with imaginary-time propagation.

are obtained by executing $\psi'(t) = \psi(t) - \sum_i \langle\psi_i|\psi(t)\rangle\psi_i$ after each time step. ψ_i represents the lower-energy eigenstates. The parameters given in Table I ensure the obtained initial state, possessing the same symmetry as the highest occupied molecular orbital (HOMO) of the target molecule, has the same ionization potential as that of the HOMO [16,43]. The initial states obtained for CO_2 and N_2 are shown in Fig. 1, respectively. The orbital of CO_2 possesses π_g symmetry with the ionization potential being 13.9 eV, and the orbital of N_2 with σ_g symmetry has the ionization potential of 15.9 eV.

For atoms, the SAE soft-core potential is in the form [46]

$$V(\mathbf{r}) = -\frac{1}{\sqrt{\mathbf{r}^2 + a^2}}, \tag{4}$$

with a being the soft-core parameter. In this work, a^2 takes the values of 0.58 and 0.38 to simulate the reference atoms, who have the same ionization potentials compared with CO_2 and N_2, respectively. Although the reference atoms are atomic models to reproduce the ionization potential of corresponding molecules, one can find real atoms with close ionization potentials to them. For $a^2 = 0.58$ the obtained ionization potential equals that of Ar, and for $a^2 = 0.38$ the obtained ionization potential is very close to that of K (15.76 eV).

Starting from the initial state, the time-dependent wave function $\psi(\mathbf{r},t)$ can be obtained via real-time propagation. To calculate the high-order-harmonic radiation, the time-dependent dipole acceleration $\ddot{\mathbf{d}}(t)$ is obtained according to the Ehrenfest theorem [47]

$$\ddot{\mathbf{d}}(t) = -\langle\psi(\mathbf{r},t)|\nabla V(\mathbf{r}) + \mathbf{E}(t)|\psi(\mathbf{r},t)\rangle. \tag{5}$$

The harmonic spectrum is then obtained from the Fourier transform of $\ddot{\mathbf{d}}(t)$,

$$\mathbf{E}_{\mathrm{XUV}} = \int \ddot{\mathbf{d}}(t)\exp(-iq\omega_0 t)dt, \tag{6}$$

$$S_q = |\mathbf{E}_{\mathrm{XUV}}|^2, \tag{7}$$

where q corresponds to the harmonic order. In the calculation we have checked the robustness of our results with the precision of initial condition computation and have found qualitatively similar results.

III. RESULT AND DISCUSSION

A. Observation of molecular HHG by CPLP

In this work small linear molecules CO_2 and N_2 are applied as a target. The molecules are aligned along the x axis in the laboratory frame and interact with the CPLP, as shown in

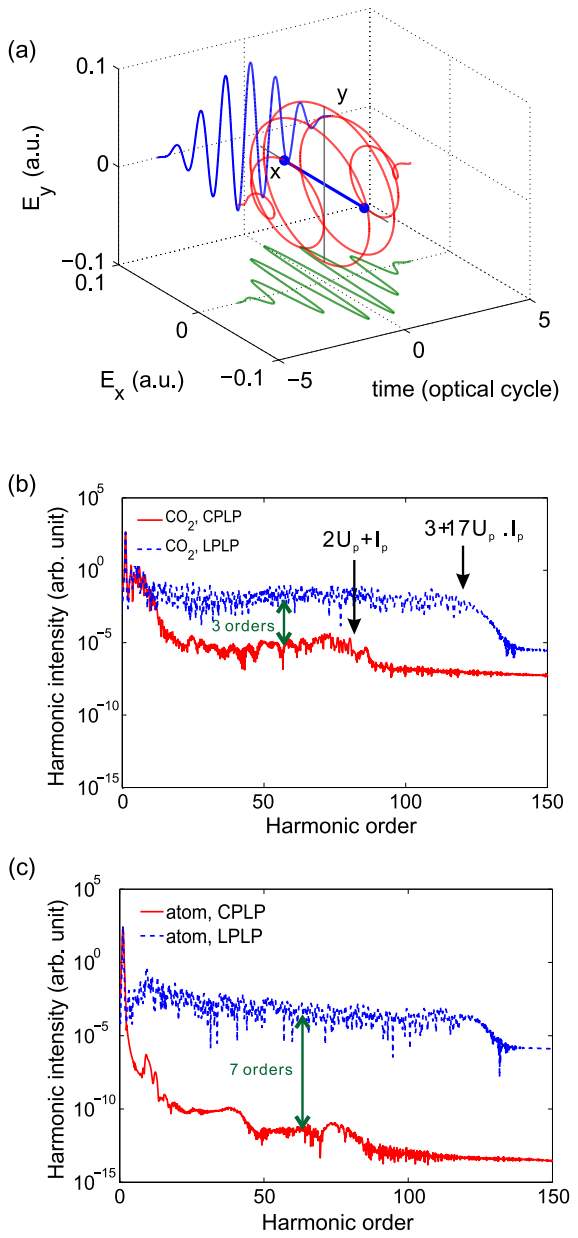

FIG. 2. (Color online) (a) Schematic for the interaction of molecules with CPLP. The 3D electric field is plotted by the red curve, the 2D projections of which are also shown in the time-E_x and time-E_y planes with green and blue curves. The molecules are aligned along the x axis in the laboratory frame. (b) Harmonic spectra from CO_2 driven by CPLP and LPLP. The intensity and wavelength of CPLP are 4×10^{14} W/cm^2 and 1300 nm, respectively. The LPLP have the same field amplitude, wavelength, and pulse duration as the CPLP. (c) Harmonic spectra from the reference atom for CO_2 driven by the same CPLP and LPLP.

Fig. 2(a). We consider a $\cos^2$ laser pulse with the full width of $T = 30$ fs:

$$E_x(t) = E_0 \cos^2\left(\frac{\pi t}{T}\right)\cos(\omega_0 t), \tag{8}$$

$$E_y(t) = E_0 \cos^2\left(\frac{\pi t}{T}\right)\sin(\omega_0 t). \tag{9}$$

We first investigate the HHG from CO_2 driven by the CPLP with intensity $I = 4 \times 10^{14}$ W/cm^2 and wavelength $\lambda = 1300$ nm. The obtained harmonic spectrum is presented in Fig. 2 (b) with the red solid curve. The harmonic spectrum of CO_2 generated by LPLP with the same field amplitude, wavelength, and pulse duration is also plotted in Fig. 2(b) with the blue dashed curve. The laser field polarizes at a 30° angle relative to the molecular axis in the LPLP case to avoid the ionization suppression due to the nodal structure of the molecular orbital [40]. It is shown that the harmonic spectrum generated by CPLP displays a typical structure as that generated by LPLP: the harmonics decrease rapidly for the low harmonic orders, then keep constant over many orders forming a plateau, and finally end abruptly at the cutoff.

As a comparison, the harmonic spectra from the reference atom generated by the same laser pulses are also presented in Fig. 2(c). Comparing Figs. 2(b) and 2(c) it is found that, with the same ionization potential, the intensities of the harmonics from CO_2 and the reference atom are in the same level for LPLP, while the harmonic intensities are far different for CPLP. The intensity of high-order harmonics generated by CPLP is about 7 orders of magnitude lower than that generated by LPLP for an atom. The intensity difference is much smaller for CO_2, which is approximately 3 orders of magnitude. Both in the CPLP case, the harmonic intensity of CO_2 is about 5 orders of magnitude higher than that of the reference atom (can also be seen in Fig. 3). These results show that the HHG driven by CPLP from the molecular target CO_2 is more efficient than that from the atom and is more easily to be observed. Although the intensity difference should be larger than that in our 2D calculation, the decrease of HHG driven by CPLP has been dramatically reduced for the molecule. Another important observation for the molecular HHG driven by CPLP is that the cutoff is located at the 81st harmonic order, which is different from that for LPLP with the same field amplitude and approximately equals $2U_p + I_p$ in photon energy [38].

To check whether these phenomena are general for the laser parameters commonly used and to uncover the mechanism of this molecular HHG, we scan the laser intensity from 2×10^{14} to 6×10^{14} W/cm^2 with fixed wavelength 1300 nm, and scan the wavelength of the laser pulse from 900 to 1500 nm with fixed intensity 4×10^{14} W/cm^2, respectively. The results are displayed in Fig. 3. The spectra of CO_2 are plotted with the red solid curves and the spectra from the reference atom are plotted with the black dotted curves. From all eight pairs of spectra, one can see the intensity of molecular spectra keeps in the same level and are all about 4–6 orders of magnitude higher than the atomic spectra. This indicates that the higher efficiency of molecular HHG is not unique for specific laser parameters, but is general for the laser pulses commonly used for HHG.

Moreover, it is shown in Fig. 3 that the positions of the cutoff increase with the driving laser intensity and the wavelength. To investigate the dependence of the cutoff position on the laser parameters in more detail, we summarize the cutoff positions with respect to different laser parameters in Table II. The cutoff is judged at the position where the spectrum begins to drop by visual inspection. Because of the irregular structure of the harmonic spectrum especially with CPLP, it is not easy to exactly point out the location of the cutoff by visual inspection.

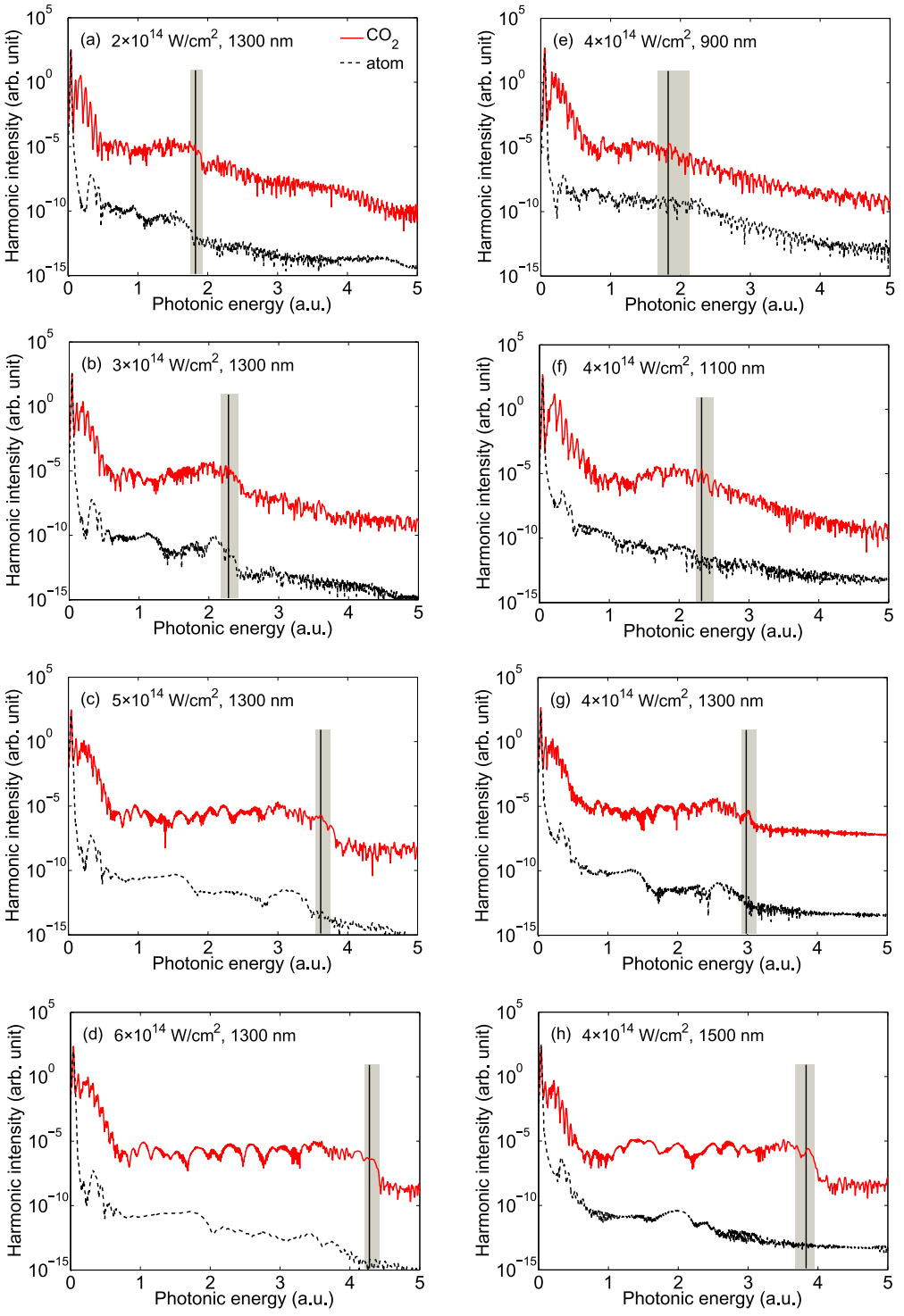

FIG. 3. (Color online) Harmonic spectra from CO_2 (red solid curves) and from the reference atom (black dashed curves) driven by CPLP with different laser parameters. In the left column, the laser wavelength is fixed to be 1300 nm, and the laser intensities are $I = 2,3,5,6 \times 10^{14}$ W/cm^2, respectively. In the right column, the laser intensity is fixed to be $I = 4 \times 10^{14}$ W/cm^2, and the laser wavelengths are 900, 1100, 1300, 1500 nm, respectively. The vertical lines label the cutoff positions and the background shadings indicate the errors as listed in Table II.

Therefore, errors for the cutoff positions are also listed in parentheses in the fourth and fifth columns in Table II. These cutoff positions and errors are labeled in Fig. 3 by the vertical lines and the background shadings, respectively. In the last column of Table II, Keldysh parameters $\gamma = \sqrt{I_p/U_p}$ are also listed, which shows that for all the laser parameters $\gamma < 1$ (i.e., in the tunneling regime).

Then we fit the observed cutoff positions in CO_2 harmonic spectra as a function of U_p, as shown in Fig. 4. The data marked by diamonds denote the results with fixed wavelength

TABLE II. Cutoff positions in photon energy with respect to different laser parameters and molecules. Errors for the cutoff positions are also listed in the parentheses in the form of (positive error/negative error).

I (W/cm^2)	λ (nm)	U_p (a.u.)	Cutoff position (a.u.)		γ	
			CO_2	N_2	CO_2	N_2
2		0.5778	1.82 (+0.11/−0.07)	1.82 (+0.14/−0.04)	0.6711	0.7158
3		0.8667	2.28 (+0.14/−0.11)	2.39 (+0.14/−0.11)	0.5512	0.5867
4	1300	1.1556	2.98 (+0.14/−0.07)	2.98 (+0.11/−0.07)	0.4802	0.5100
5		1.4445	3.61 (+0.14/−0.07)	3.58 (+0.14/−0.07)	0.4320	0.4579
6		1.7335	4.28 (+0.14/−0.07)	4.31 (+0.07/−0.07)	0.3966	0.4195
	900	0.5539	1.82 (+0.30/−0.15)	1.82 (+0.15/−0.10)	0.6777	0.7261
	1100	0.8274	2.32 (+0.17/−0.08)	2.40 (+0.17/−0.01)	0.5548	0.5947
4	1300	1.1556	2.98 (+0.14/−0.07)	2.98 (+0.11/−0.07)	0.4802	0.5100
	1500	1.5386	3.83 (+0.12/−0.15)	3.86 (+0.12/−0.15)	0.4107	0.4383

λ = 1300 nm, and those marked by triangles denote the data with fixed intensity $I = 4 \times 10^{14}$ W/cm^2. The corresponding laser parameters are labeled beside the marks in the form of [I ($\times 10^{14}$W/cm^2), λ (nm)]. Error bars corresponding to the errors for the cutoff positions are also shown in the figure with the short black lines. It is found that the cutoff data are well fitted by a straight line $E_{\text{cutoff}} = 2.15U_p + 0.515$ (E_{cutoff} is the cutoff position in photon energy).

The HOMO of CO_2 is an antibounding orbital with π_g symmetry. Differently, the HOMO of N_2 is a bounding orbital with σ_g symmetry and has a higher ionization potential. In Fig. 5(a) the harmonic spectra from N_2 generated by CPLP and LPLP are displayed. The driving pulses are the same as those in Fig. 2(b). The harmonic spectra from the reference atom generated by the same CPLP and LPLP are also presented in Fig. 5(b). Similarly, it is found that the intensity difference between the high-order harmonics generated by CPLP and LPLP is much smaller for N_2 than for the reference atom,

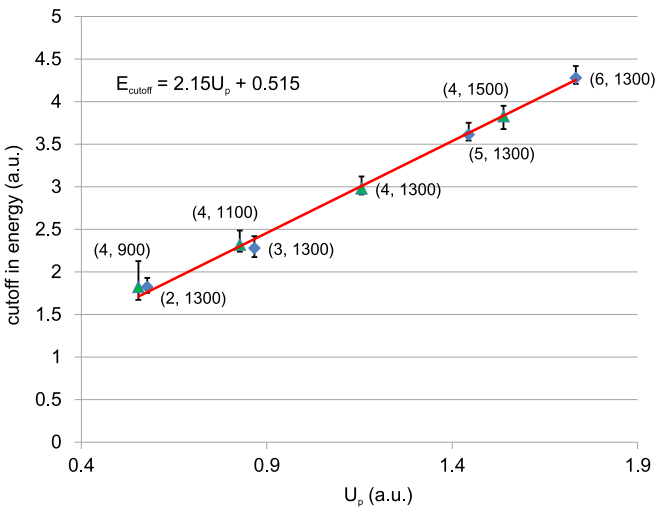

FIG. 4. (Color online) Linear fit of the cutoff positions with respect to different laser parameters for CO_2. The horizontal coordinate is $U_p = E_0^2/4\omega_0^2$. The data marked by diamonds denote the results with fixed wavelength λ = 1300 nm, and those marked by triangles denote the data with fixed intensity $I = 4 \times 10^{14}$ W/cm^2. The corresponding laser parameters are labeled beside the marks in the form of [I ($\times 10^{14}$W/cm^2), λ (nm)].

which is about 3 orders of magnitude for N_2 and 7 orders of magnitude for the atom. Both in the CPLP case, the intensity of molecular high-order harmonics is 3–4 orders of magnitude higher than that of the reference atom. We also scan the laser parameters and summarize the cutoff positions in Table II. The linear fit of these data are presented in Fig. 5(c), which shows that the cutoff position depends on U_p by $E_{\text{cutoff}} = 2.12U_p + 0.585$. In the spectra of N_2, one can see a peak at the 63rd harmonic order, which is 59.84 eV in energy. The position of this peak does not change in energy for different laser parameters and 59.84 eV equals the energy gap between the applied initial state of N_2 and the lowest-energy eigenstate. Therefore, this peak should be the artificial "resonant peak" due to the SAE model. However, it does not influence the main performance of the spectra, such as the intensity and the cutoff, and the discussion on the mechanism of HHG.

In both cases of CO_2 and N_2, the cutoff scales as $E_{\text{cutoff}} \approx 2U_p + I_p$. This is consistent with the results from TDSE calculation and the calculation based on the traditional semiclassical recollision model in [38], where the HHG by CPLP from atoms with pure ground state is discussed.

It is worth noting that in [37], where an excited initial condition is considered, the cutoff follows $3.17U_p + I_p$ from the TDSE calculation. And both the upper and lower cutoffs can be well predicted by the calculation based on the recolliding periodic orbits (RPO) analysis [36]. We attribute the difference between the two found cutoff laws to the fact that different definitions of cutoff are used. In our work, the cutoff is judged where the spectrum begins to drop. And in [37], the upper cutoff is judged where the spectrum has already vanished. Because of this, two "different" cutoff laws are found. If one uses the cutoff definition in our work to the TDSE results in [37], it is shown that the $2U_p + I_p$ cutoff law also works well. Therefore, there is actually no contradiction between the two concluded cutoff laws.

The position of cutoff depends linearly on U_p, which means that it depends linearly on E_0^2. Previous works have shown that in the HHG due to a bound-bound mechanism the cutoff position depends linearly on E_0 [28,30], which is different from our results. This proves that the molecular HHG found in this work is different from the known "symmetry-allowed harmonics". On the other hand, the agreement between the scaling law of the cutoff position and the prediction based on

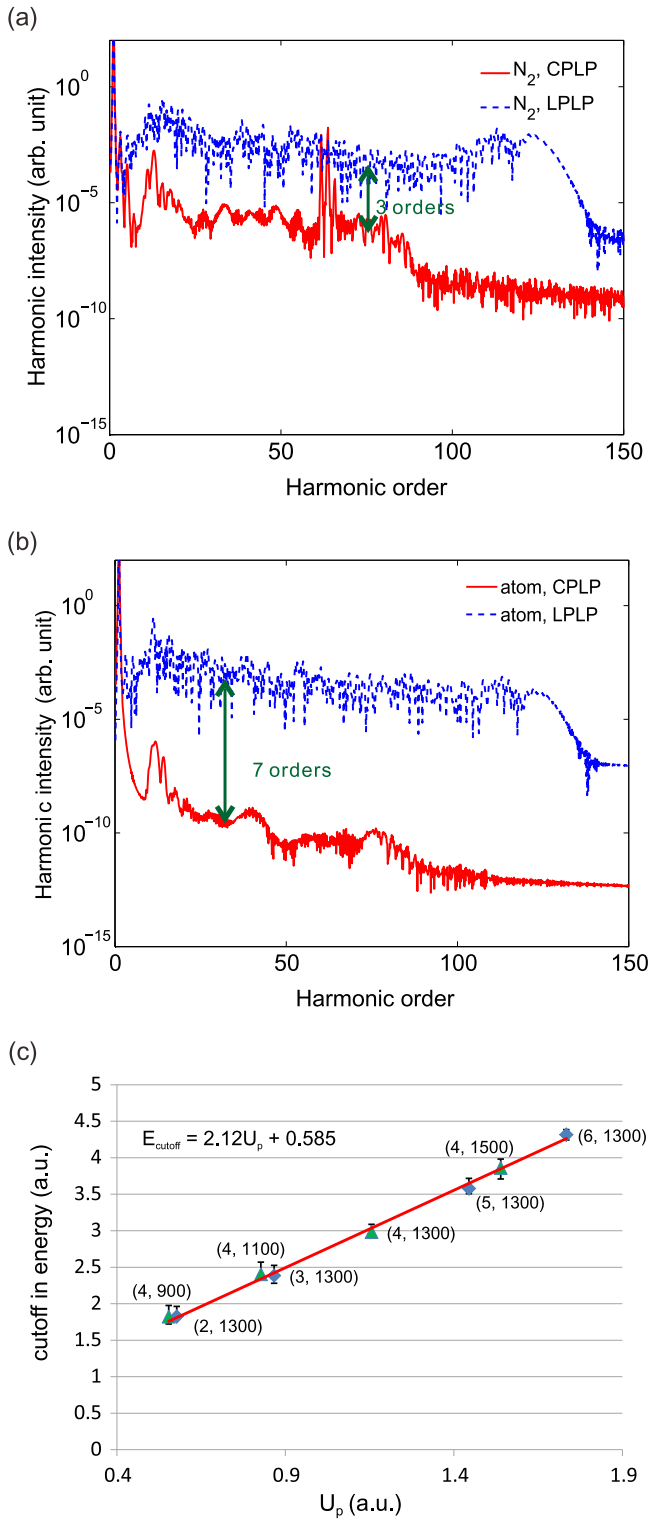

FIG. 5. (Color online) (a) Harmonic spectra from N_2 driven by the same CPLP and LPLP as those in Fig. 2(b). (b) Harmonic spectra from the reference atom for N_2 driven by the same CPLP and LPLP, respectively. (c) Linear fit of the cutoff positions with respect to different laser parameters for N_2. The definitions of the symbols are the same as in Fig. 4.

the semiclassical recollision picture implies that the HHG can be due to the recollision mechanism. A more sufficient and direct proof for this conclusion should be an observation of the recollision. This will be shown latter in Fig. 8 when the recolliding trajectories are calculated.

B. Analysis on the higher efficiency of molecular HHG by CPLP

The atomic HHG with CPLP is usually considered impossible (very inefficient). In [37] it was proposed that such HHG can be made possible (more efficient) by considering an excited initial wave packet composed of ground and excited states. In our calculation, the atomic HHG is calculated solely from the ground state. This explains the fact that the atomic harmonic signal obtained in this work is very weak. While in the case of molecular HHG, the wave packet is also composed of only the HOMO eigenstate, but the HHG efficiency is much higher. This implies there are some other reasons that make the HHG more efficient. In the following we will analyze the HHG process and discuss the origin of the higher efficiency of molecular HHG driven by CPLP. According to the semiclassical recollision model, the HHG consists of three steps: ionization, acceleration, and recombination.

First, we examine the ionization step for both molecular and atomic cases. We evaluate the ionization probability P during the interaction of the target with CPLP in two ways.

(1) In each time step of TDSE propagation,

$$P_1(t) = 1 - \sum_{i=1}^{11} |\langle \psi_i | \psi(t) \rangle|^2, \tag{10}$$

where ψ_i is the ith lowest-energy field-free eigenstate obtained via the imaginary-time propagation.

(2) In each time step of TDSE propagation,

$$P_2(t) = 1 - \langle \psi_{|x|,|y|<20}(t) | \psi_{|x|,|y|<20}(t) \rangle, \tag{11}$$

i.e., the probability is calculated by subtracting the density distribution in a box of 20 a.u. $\times$ 20 a.u. in space.

The calculated ionization probabilities P_1 and P_2 are presented in Fig. 6. It is shown that, by using the two ways, P_1 and P_2 give nearly identical results. Figures 6(a) and 6(b) display the results for CO_2 and N_2 compared with the respective reference atoms. It is found that the ionization probability is lower for molecules than atoms. Therefore, the higher efficiency does not result from higher ionization probability.

As the bound states of atoms are more highly ionized than the those of molecules, to check whether the effect of bound state depletion plays a role, we perform time-windowed harmonic analysis [48] for the HHG from CO_2, N_2, and the reference atoms. Figure 7 shows the time-windowed harmonic analysis results for the laser parameters of $I = 4 \times 10^{14}$ W/cm^2 and $\lambda = 800$ nm, i.e., the time-frequency distributions in Figs. 6(a)–6(d) correspond to the harmonic spectra shown in Figs. 2(b), 2(c), 5(a), and 5(b) and the ionization probability calculation in Fig. 6, respectively. It is shown that the variations of the HHG radiation with time are similar for the molecules and the respective atoms. The harmonic intensities for atoms are smaller than those for the corresponding molecules uniformly through the whole pulse duration. No abrupt elimination of the atomic HHG compared with the molecular HHG is observed. This result indicates that

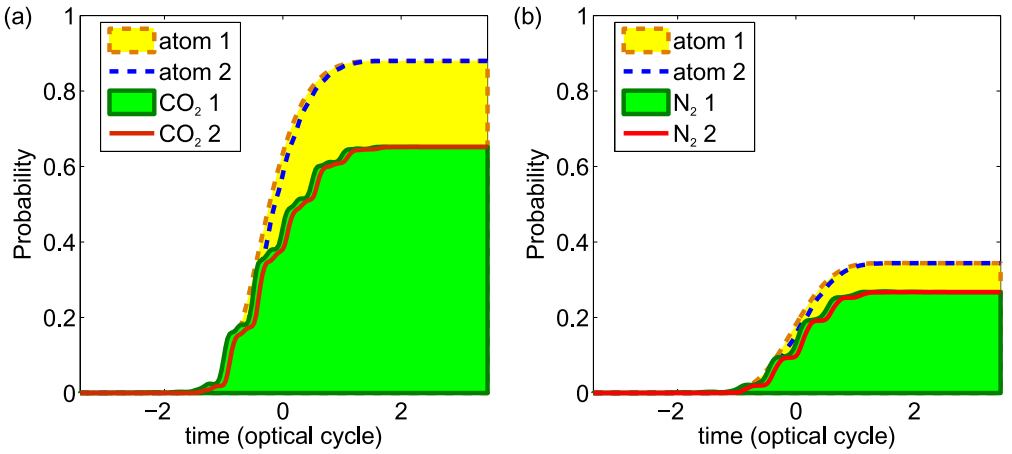

FIG. 6. (Color online) Ionization probabilities for (a) CO_2 and (b) N_2 (solid curves and edges) compared with those for the respective reference atoms (dashed curves and edges) with laser intensity and wavelength $I = 4 \times 10^{14}$ W/cm^2 and $\lambda = 800$ nm, respectively. The numbers 1 or 2 in the legends denote that the ionization probabilities are calculated according to the formulas in Eq. (10) or (11), respectively.

the bound state depletion effect does not play a role on the higher efficiency for molecular HHG.

Next, we study the acceleration and recombination steps employing the semiclassical model similar to [38,49–51]. Since a multicycle laser pulse is applied in the TDSE calculation, we neglect the effect of envelope by assuming the envelope $f(t) \equiv 1$ in the following calculation for simplicity. The intensity and wavelength of the laser pulse are $I = 4 \times 10^{14}$ W/cm^2 and 1300 nm, respectively. To emulate the evolution of the ionized electron, an 10^5 ensemble of trajectories are launched at a certain time t_0 with different initial conditions. Within the tunneling regime, the initial position $\mathbf{r}_0$ is determined by finding the tunnel exit satisfying

$$V(\mathbf{r}_0) + \mathbf{r}_0 \cdot \mathbf{E}(t_0) = -I_p. \tag{12}$$

The potential V is given in Eqs. (3) and (4) for different target system. For some laser parameters, it is found that the intensity is a little higher than the barrier suppression

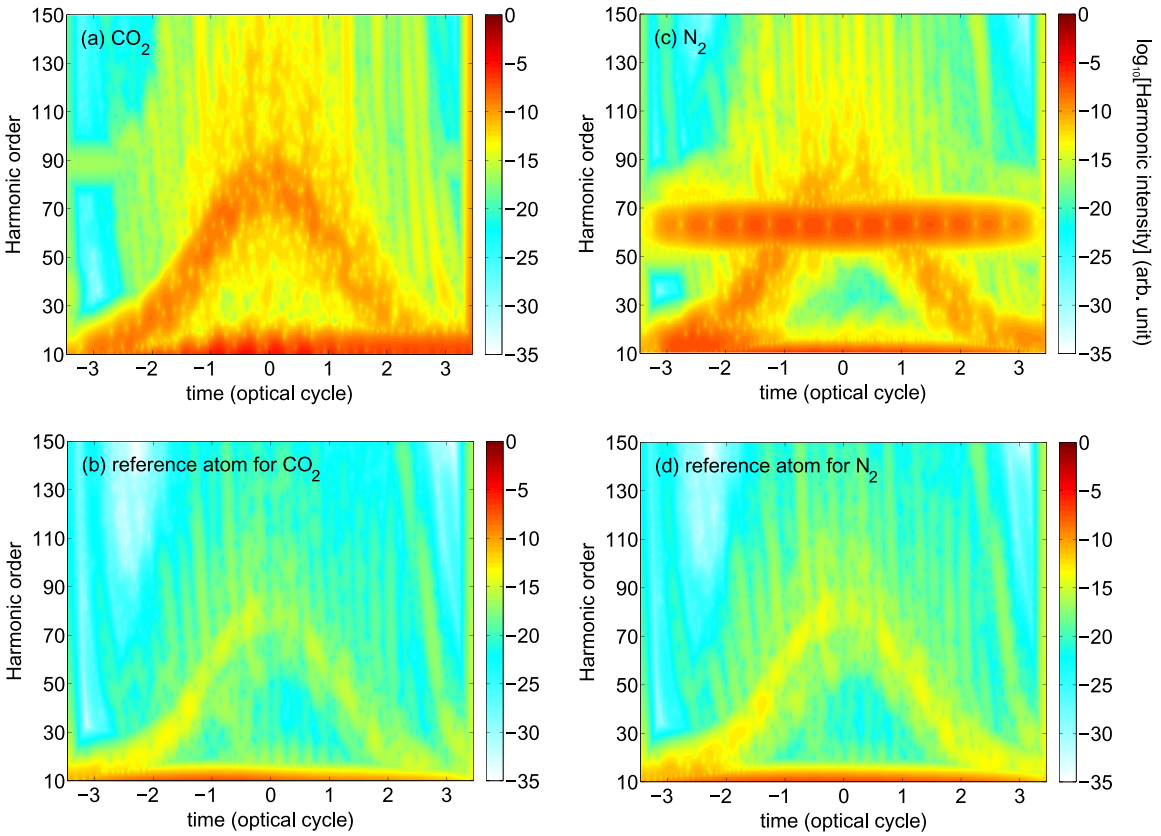

FIG. 7. (Color online) Time-windowed harmonic analysis for the HHG from CO_2, N_2, and the reference atoms with laser intensity and wavelength $I = 4 \times 10^{14}$ W/cm^2 and $\lambda = 800$ nm, respectively.

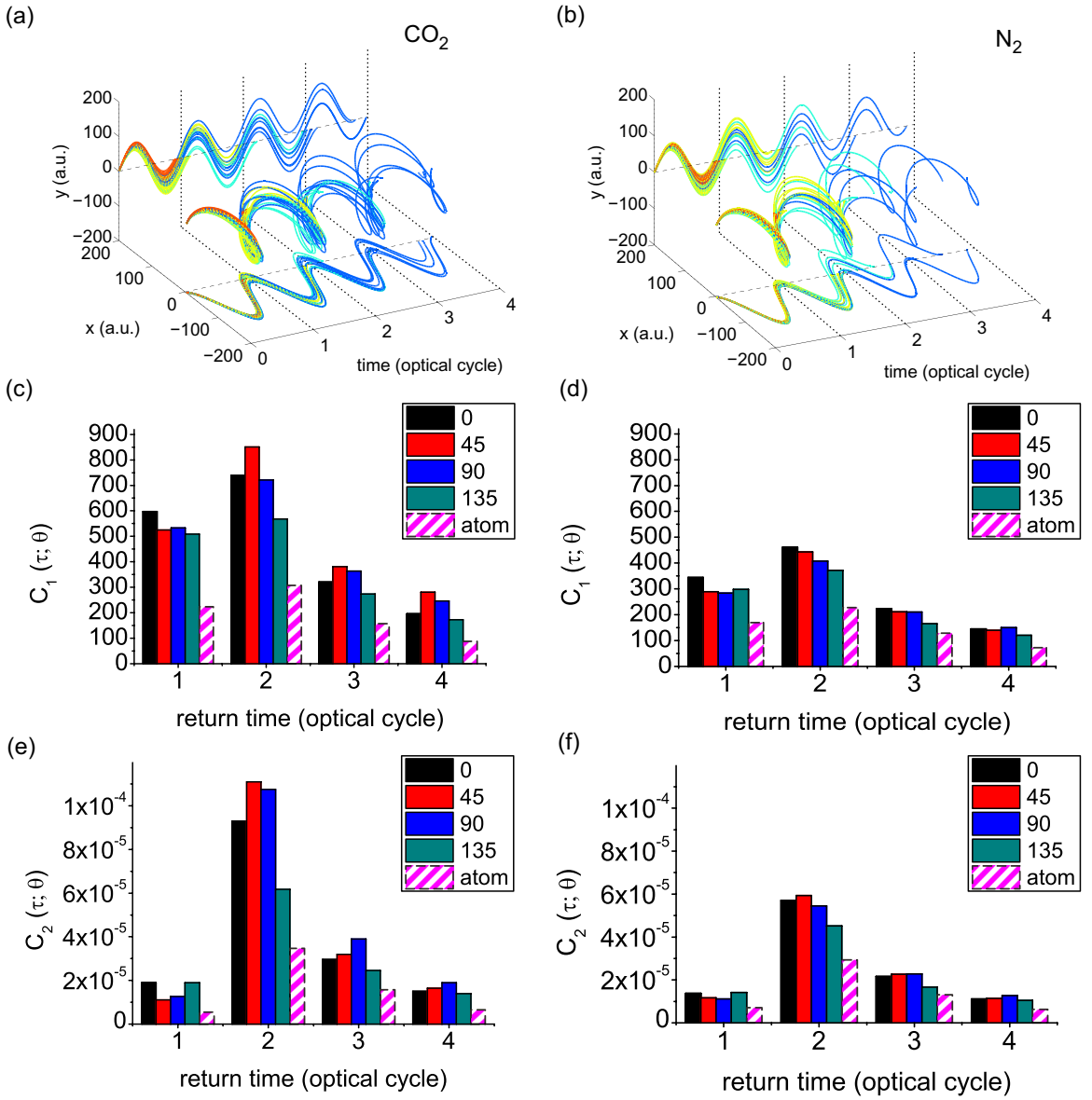

FIG. 8. (Color online) (a) and (b) Classical recolliding trajectories of the ionized electrons at $\theta = 0$ for CO_2 and N_2. Different trajectories are plotted with different colors depending on the times they return to the core. Red trajectories return earliest and blue trajectories return last. The 2D projections of the trajectories are also shown in the time-x and time-y planes, respectively. (c)–(f) Counts of recollisions within different optical cycles for $\theta = 0$, 45, 90, 135 deg and for the reference atoms, respectively. The left column shows the results for CO_2 and the right column presents the results for N_2.

intensity, where Eq. (12) does not have a real solution. In these cases, the initial position is determined by finding the spot where the electron goes over the maximum of the potential. The initial perpendicular momentum $p_\perp$ ranges from -4 to 4 a.u. [perpendicular to $\mathbf{E}(t_0)$] in steps of 0.008 a.u. and initial longitude momentum ranges $p_\parallel$ from -0.4 to 0 a.u. [along $\mathbf{E}(t_0)$] in steps of 0.004 a.u.

Then, the evolution of the ionized electron is described by the classical equation

$$\frac{d^2\mathbf{r}}{dt^2} = -\nabla V(\mathbf{r}) - \mathbf{E}(t) \tag{13}$$

until it recollides with the core or it has evolved for more than four optical cycles. The recollision is judged when the electron approaches the nucleus within a distance of 1 a.u.

For different initial time t_0, when the angle between the instantaneous electric field and the x axis is θ, we perform the semiclassical calculation and count the number of return electrons C_1 for the molecule and the corresponding reference atom. Moreover, according to [52], each trajectory is weighted by

$$w(p_\parallel, p_\perp) \sim \exp\{-[2I_p + p_\perp^2 + (p_\parallel - E/\omega)^2]^{2/3}\}. \tag{14}$$

Therefore, we take into account the weights associated with different initial moments and record the weighted count of recollision C_2.

In Figs. 8(a) and 8(b), typical recolliding trajectories of electrons ionized at $\theta = 0$ for CO_2 and N_2 are obtained with this semiclassical model. The 2D projections of the trajectories

are also shown in the time-x and time-y planes, respectively. To make it easier to distinguish the trajectories, different trajectories are plotted with different colors depending on the times they return to the core. Red trajectories return earliest and blue trajectories return last. As shown in the figures, the ionized electrons may be accelerated by the electric field around the core for several optical cycles and then recombine to the core. This is a direct observation of the recollision in the HHG process driven by CPLP, and indicates that the observed HHG by CPLP is due to the recollision mechanism combining with the preceding discussions.

For the insight of this process, we count the recollisions within different optical cycles $C_1(\tau;\theta)$ and $C_2(\tau;\theta)$ for $\theta = 0$, 45, 90, 135 deg, respectively, as shown in Figs. 8(c)–8(f). The left column shows the results for CO_2 and the right column presents the results for N_2. τ is the time delay between ionization and recollision. The results for the respective reference atoms are also shown with bars filled with purple stripes. It is well known that in the acceleration step, the quantum diffusion effect plays an important role on the HHG efficiency. The longer the acceleration period τ is, the weaker the HHG is. From the statistics of both $C_1(\tau;\theta)$ and $C_2(\tau;\theta)$, it is found that most recollision occurs in the second optical cycle. The counts then decrease with the return time increasing. This distribution of the counts as functions of return time is nearly the same for both molecules and atoms. This means that the different HHG efficiency is not due to different acceleration processes in the acceleration step.

However, one can see that all the C_1 and C_2 are higher for molecules than those for respective reference atoms, which implies a higher recollision probability for molecules. We then calculate $C_1(\theta)$ and $C_2(\theta)$ as functions of θ from 0 to 150 deg in a smaller step of 30 deg, and present the ratios of the counts for CO_2 and N_2 to those for reference atoms in Figs. 9(a) and 9(b), respectively. The results show that, in the recombination step, the recollision probability is about 2.5 times and nearly 2 times higher for CO_2 and N_2 than that for the reference atom. This higher probability results from two reasons. One is there are more cores for the electrons to recollide with in a molecule system. The other one is that the Coulomb focusing effect [53] is more effective because of the multicenter structure of the molecular potential.

We have analyzed the three steps in the process of HHG from small molecules and atoms step by step. All the results and discussions have shown that the ionization and acceleration steps do not lead to the higher efficiency of molecular HHG, which suggests that this higher efficiency for molecular HHG driven by CPLP is mainly contributed in the recombination step. Moreover, the semiclassical calculation have qualitatively explained that the higher efficiency should be at least partly due to the higher recollision probability of continuum electrons. Owning to the multicenter structure of molecules, the continuum electrons return to the vicinity of the cores and recombine to generate harmonic photons more easily. Both the larger dimension and the more effective Coulomb focusing effect play roles. However, the semiclassical model cannot explain the TDSE results exactly. This is because the HHG by CPLP is a complex process and many quantum effects are missing in this model where the electrons and cores are only treated as classical particles. For example, the recombination probability is not only dependent on the recollision probability in the aspect of the classical picture. It will also be determined by the symmetry of the molecular orbitals and the recombination direction. Besides, there might also be some other effects not considered having influence on the HHG efficiency. The bound-bound transition effect can be excluded for the higher intensity of the molecular HHG. Because the cutoff of the high-order harmonics due to the bound-bound transition effect is different from that due to the recollision effect, while the observed cutoff in this work is just consistent with the recollision model and no dual-plateau structure (implying both mechanisms may contribute to the HHG) is found in the molecular harmonic spectra.

IV. CONCLUSION

HHG from small linear molecules driven by intense CPLP is investigated in this paper. It is found that the harmonic intensity is several orders of magnitude higher (or much less decreased compared with the harmonic intensity by using LPLP) than that from the reference atom with an equal ionization potential. By varying the laser intensity and wavelength, the cutoff of the harmonic spectra depends on the laser parameters with the relation $E_{\text{cutoff}} \approx 2U_p + I_p$, which is consistent with the semiclassical recollision model. Moreover, the "recollision" is observed by obtaining the recolliding trajectories with semiclassical calculation. These results indicate that this kind of molecular HHG originates from the recollision mechanism. Then, by analyzing the HHG process, it is shown that the

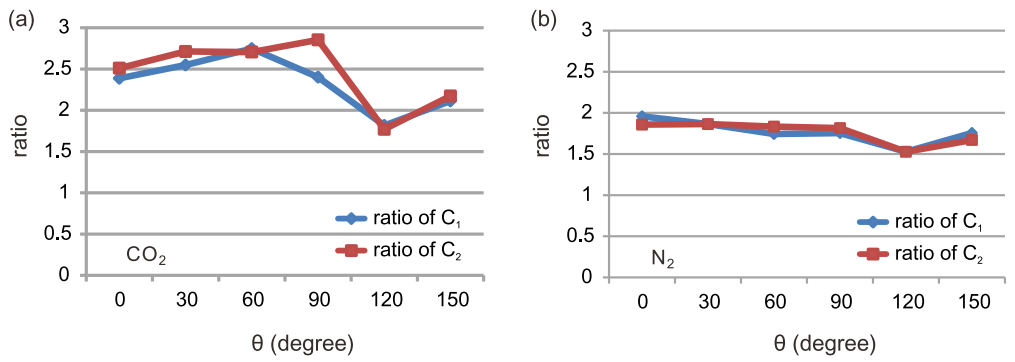

FIG. 9. (Color online) Ratios of the counts for (a) CO_2 and (b) N_2 to those for respective reference atoms.

higher efficiency of the molecular HHG is mainly contributed in the recombination step and at least partly results from the higher recollision probability of continuum electrons due to the multicenter structure of molecules.

Investigations on molecular HHG driven by CPLP will stimulate new potential applications. For example, it can provide a way to generate circularly polarized ultrafast XUV pulses [7–9,37]. Moreover, considering that the HHG efficiency is still lower compared with that by LPLP, the more significant benefit for this kind of HHG is one can utilize the unique recollision scheme under a circularly polarized laser field for different purposes. For instance, this HHG process offers an ideal framework for the study of strong-field dynamics [37]. Moreover, as the CPLP has already shown its great power in the application of (one-shot) imaging or structure detection of molecules [39–42], the HHG by CPLP can be potentially utilized for the imaging and detection of molecules with an all-optical method.

ACKNOWLEDGMENTS

This work was supported by the National Natural Science Foundation of China under Grants No. 11234004, No. 11404123, and No. 61275126 and the 973 Program of China under Grant No. 2011CB808103. Numerical simulations presented in this paper were carried out using the High Performance Computing Center experimental testbed in SCTS/CGCL (see http://grid.hust.edu.cn/hpcc).

[1] Y. Mairesse, A. de Bohan, L. J. Frasinski, H. Merdji, L. C. Dinu, P. Monchicourt, P. Breger, M. Kovačev, R. Taïeb, B. Carré, H. G. Muller, P. Agostini, and P. Salières, Science **302**, 1540 (2003).
[2] E. Goulielmakis, M. Schultze, M. Hofstetter, V. S. Yakovlev, J. Gagnon, M. Uiberacker, A. L. Aquila, E. M. Gullikson, D. T. Attwood, R. Kienberger, F. Krausz, and U. Kleineberg, Science **320**, 1614 (2008).
[3] P. Lan, P. Lu, W. Cao, Y. Li, and X. Wang, Phys. Rev. A **76**, 011402 (2007).
[4] V. Strelkov, Phys. Rev. Lett. **104**, 123901 (2010).
[5] A. Etches and L. B. Madsen, J. Phys. B: At. Mol. Opt. Phys. **43**, 155602 (2010).
[6] E. J. Takahashi, P. Lan, O. D. Mucke, Y. Nabekawa, and K. Midorikawa, Nat. Commun. **4**, 2691 (2013).
[7] D. B. Milošević, W. Becker, and R. Kopold, Phys. Rev. A **61**, 063403 (2000).
[8] K. J. Yuan and A. D. Bandrauk, J. Phys. B: At. Mol. Opt. Phys. **45**, 074001 (2012).
[9] K. J. Yuan and A. D. Bandrauk, Phys. Rev. Lett. **110**, 023003 (2013).
[10] M. Lein, J. Phys. B: At. Mol. Opt. Phys. **40**, R135 (2007).
[11] O. Smirnova, Y. Mairesse, S. Patchkovskii, N. Dudovich, D. Villeneuve, P. Corkum, and M. Y. Ivanov, Nature **460**, 972 (2009).
[12] S. Haessler, J. Caillat, and P. Salières, J. Phys. B: At. Mol. Opt. Phys. **44**, 203001 (2011).
[13] J. Itatani, J. Levesque, D. Zeidler, H. Niikura, H. Pépin, J. C. Kieffer, P. B. Corkum, and D. M. Villeneuve, Nature (London) **432**, 867 (2004).
[14] S. Haessler, J. Caillat, W. Boutu, and C. Giovanetti-Teixeira, Nat. Phys. **6**, 200 (2010).
[15] C. Vozzi, M. Negro, F. Calegari, G. Sansone, M. Nisoli, S. De Silvestri, and S. Stagira, Nat. Phys. **7**, 822 (2011).
[16] Y. J. Chen, L. B. Fu, and J. Liu, Phys. Rev. Lett. **111**, 073902 (2013).
[17] Y. Li, X. Zhu, P. Lan, Q. Zhang, M. Qin, and P. Lu, Phys. Rev. A **89**, 045401 (2014); X. Zhu, M. Qin, Q. Zhang, Y. Li, Z. Xu, and P. Lu, Opt. Express **21**, 5255 (2013); X. Zhu, M. Qin, Y. Li, Q. Zhang, Z. Xu, and P. Lu, Phys. Rev. A **87**, 045402 (2013).
[18] F. Brunel, Phys. Rev. Lett. **59**, 52 (1987).
[19] P. B. Corkum, Phys. Rev. Lett **71**, 1994 (1993).
[20] K. J. Schafer, B. Yang, L. F. DiMauro, and K. C. Kulander, Phys. Rev. Lett. **70**, 1599 (1993).
[21] J. J. Macklin, J. D. Kmetec, and C. L. Gordon III, Phys. Rev. Lett. **70**, 766 (1993).
[22] A. L'Huillier and P. Balcou, Phys. Rev. Lett. **70**, 774 (1993).
[23] K. S. Budil, P. Salières, A. L'Huillier, T. Ditmire, and M. D. Perry, Phys. Rev. A **48**, R3437 (1993).
[24] M. Möller, Y. Cheng, S. D. Khan, B. Zhao, K. Zhao, M. Chini, G. G. Paulus, and Z. Chang, Phys. Rev. A **86**, 011401 (2012).
[25] Y. Li, X. Zhu, Q. Zhang, M. Qin, and P. Lu, Opt. Express **21**, 4896 (2013); X. Zhu, M. Qin, Q. Zhang, W. Hong, Z. Xu, and P. Lu, *ibid.* **20**, 16275 (2012).
[26] O. E. Alon, V. Averbukh, and N. Moiseyev, Phys. Rev. Lett. **80**, 3743 (1998).
[27] O. E. Alon, V. Averbukh, and N. Moiseyev, Phys. Rev. Lett. **85**, 5218 (2000).
[28] V. Averbukh, O. E. Alon, and N. Moiseyev, Phys. Rev. A **64**, 033411 (2001).
[29] R. Baer, D. Neuhauser, P. R. Žďánská, and N. Moiseyev, Phys. Rev. A **68**, 043406 (2003).
[30] P. Žďánská, V. Averbukh, and N. Moiseyev, J. Chem. Phys. **118**, 8726 (2003).
[31] I. Bâldea, A. K. Gupta, L. S. Cederbaum, and N. Moiseyev, Phys. Rev. B **69**, 245311 (2004).
[32] P. Moreno, L. Plaja, and L. Roso, J. Opt. Soc. Am. B **13**, 430 (1996); Phys. Rev. A **55**, R1593 (1997).
[33] A. D. Bandrauk, S. Barmaki, and G. L. Kamta, Phys. Rev. Lett. **98**, 013001 (2007).
[34] Q. Zhang, P. Lu, W. Hong, Q. Liao, P. Lan, and X. Wang, Phys. Rev. A **79**, 053406 (2009).
[35] F. Mauger, C. Chandre, and T. Uzer, Phys. Rev. Lett. **105**, 083002 (2010).
[36] A. Kamor, F. Mauger, C. Chandre, and T. Uzer, Phys. Rev. Lett. **110**, 253002 (2013).
[37] F. Mauger, A. D. Bandrauk, A. Kamor, T. Uzer, and C. Chandre, J. Phys. B: At. Mol. Opt. Phys. **47**, 041001 (2014).
[38] F.-M. Guo, G. Chen, J.-G. Chen, S.-Y. Li, and Y.-J. Yang, Chin. Phys. B **22**, 023204 (2013).
[39] X. Zhu, Q. Zhang, W. Hong, P. Lu, and Z. Xu, Opt. Express **19**, 13722 (2011).
[40] J. Maurer, D. Dimitrovski, L. Christensen, L. B. Madsen, and H. Stapelfeldt, Phys. Rev. Lett. **109**, 123001 (2012).
[41] I. Dreissigacker and M. Lein, Phys. Rev. A **89**, 053406 (2014).

[42] I. Petersen, J. Henkel, and M. Lein, Phys. Rev. Lett. **114**, 103004 (2015).
[43] M. Peters, T. T. Nguyen-Dang, E. Charron, A. Keller, and O. Atabek, Phys. Rev. A **85**, 053417 (2012).
[44] M. D. Feit, J. A. Fleck, Jr., and A. Steiger, J. Comput. Phys. **47**, 412 (1982).
[45] X.-B. Bian, Phys. Rev. A **90**, 033403 (2014).
[46] J. Javanainen, J. H. Eberly, and Q. Su, Phys. Rev. A **38**, 3430 (1988).
[47] K. Burnett, V. C. Reed, J. Cooper, and P. L. Knight, Phys. Rev. A **45**, 3347 (1992).
[48] C. C. Chirilă, I. Dreissigacker, E. V. van der Zwan, and M. Lein, Phys. Rev. A **81**, 033412 (2010).
[49] K. Doblhoff-Dier, K. I. Dimitriou, A. Staudte, and S. Gräfe, Phys. Rev. A **88**, 033411 (2013).
[50] L. B. Fu, J. Liu, J. Chen, and S. G. Chen, Phys. Rev. A **63**, 043416 (2001).
[51] Y. Zhou, C. Huang, Q. Liao, and P. Lu, Phys. Rev. Lett. **109**, 053004 (2012).
[52] N. B. Delone and V. P. Krainov, J. Opt. Soc. Am. B **8**, 1207 (1991).
[53] T. Brabec, M. Y. Ivanov, and P. B. Corkum, Phys. Rev. A **54**, R2551 (1996); K. J. Yuan and A. D. Bandrauk, *ibid.* **80**, 053404 (2009); M. V. Frolov, N. L. Manakov, T. S. Sarantseva, M. Yu. Emelin, M. Yu. Ryabikin, and A. F. Starace, Phys. Rev. Lett. **102**, 243901 (2009).